

Contents lists available at ScienceDirect

Nuclear Inst. and Methods in Physics Research, A

journal homepage: www.elsevier.com/locate/nima



Temperature-dependent charge barrier height of amorphous germanium contact detector



Rajendra Panth, Wenzhao Wei, Dongming Mei*, Jing Liu, Sanjay Bhattarai, Hao Mei, Mathbar Raut, Pramod Acharya, Kyler Kooi, Guojian Wang

Physics Department, University of South Dakota, 414 E. Clark Street, Vermillion, 57069, SD, USA

ARTICLE INFO

Keywords: Germanium detector Amorphous germanium contacts Charge barrier height Barrier height inhomogeneity

ABSTRACT

The exploration of germanium (Ge) detectors with amorphous Ge (a-Ge) contacts has drawn attention to the searches for rare-event physics such as dark matter and neutrinoless double-beta decay. The charge barrier height (CBH) of the a-Ge contacts deposited on the detector surface is crucial to suppress the leakage current of the detector in order to achieve a low-energy detection threshold and high-energy resolution. The temperature-dependent CBH of a-Ge contacts for three Ge detectors is analyzed to study the bulk leakage current (BLC) characteristics. The detectors were fabricated at the University of South Dakota using homegrown crystals. The CBH is determined from the BLC when the detectors are operated in the reverse bias mode with a guardring structure, which separates the BLC from the surface leakage current (SLC). The results show that CBH is temperature dependent. The direct relation of the CBH variation to temperature is related to the barrier inhomogeneities created on the interface of a-Ge and crystalline Ge. The inhomogeneities that occur at the interface were analyzed using the Gaussian distribution model for three detectors.

1. Introduction

Ge detectors with a large electron/hole barrier height are required to obtain a low leakage current, which is thermally generated in the contact materials. Ge detectors are widely used for γ -ray spectroscopy [1–4], rare-event physics searches such as neutrinoless double-beta $(0\nu\beta\beta)$ decay [5–7] and dark matter [8–11], as well as astroparticle physics [12], medical imaging [13] and homeland security [14]. Ge has a relatively small energy band-gap (0.67 eV at room temperature) compared to other semiconductors. Thermal phonons can excite electrons into the conduction band and cause too much noise if Ge detectors are operated at room temperature. Operating Ge detectors at cryogenic temperature reduces thermal noise and hence allows the detectors to perform energy spectroscopy. Low energy band-gap and high mobility of charge carriers in Ge provide excellent energy resolution.

Amorphous Ge (a-Ge) is one of the passivation materials used to make charge blocking contacts for Ge detectors. Three advantages make a-Ge contacts attractive for Ge detectors. One is that a-Ge contacts provide bipolar blocking for charge carriers and hence the fabrication process is simpler with only a sputtering machine unlike traditional Ge detectors made with lithium diffused contacts and boron implanted contacts, which require two different machines. The second advantage is that an a-Ge contact is a layer of a-Ge coated on the surface of Ge detector and hence maximizes the sensitive volume of the detector in contrast to a lithium diffused detector that creates a dead layer as well

as a transient layer, which decrease the sensitive volume. Lastly, the contacts can be easily segmented in an a-Ge coated detector as studied by Luke and Amman [1,15-17]. The interface between a-Ge contact and crystalline Ge creates a charge barrier height (CBH), which provides bipolar blocking for the injection of holes or electrons, depending on the sign of the applied bias voltage. The bulk leakage current (BLC) of a detector depends on the CBH of the rectifying contacts. The nature of CBH formed at the interface of a-Ge and crystalline Ge demonstrates its ability to block injection charges from the surface. However, the characterization of CBH cannot be just to perform the I-V characteristics at a given temperature. To study the conduction mechanism related to the injection of charges, temperature dependent I-V measurements are required. The applicability of Ge detector coated with a-Ge ranges from mK to 130 K. Thus, understanding the nature of CBH formation at the interface is of great importance on improving the process parameters used for the deposition of a-Ge layer since the mechanism of charge generation in the a-Ge contact layer is governed by thermionic emission. It is expected that the fluctuation of CBH with respect to temperature can be used to study the inhomogeneity of a-Ge contacts created on the crystalline surface. The inhomogeneity is related to the fabrication process, which can be improved when multiple detectors are used in this study.

Several papers have been published on the investigation of the CBH of rectifying contacts by studying the current-voltage (I-V) or

E-mail address: Dongming.Mei@usd.edu (D. Mei).

^{*} Corresponding author.

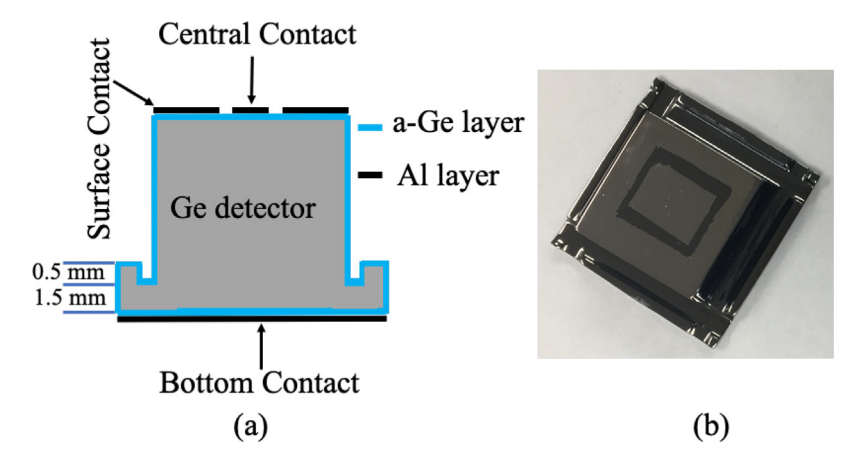


Fig. 1. (a) Schematic representation of a Ge detector with a guard-ring structure. (b) A guard-ring Ge detector fabricated at USD.

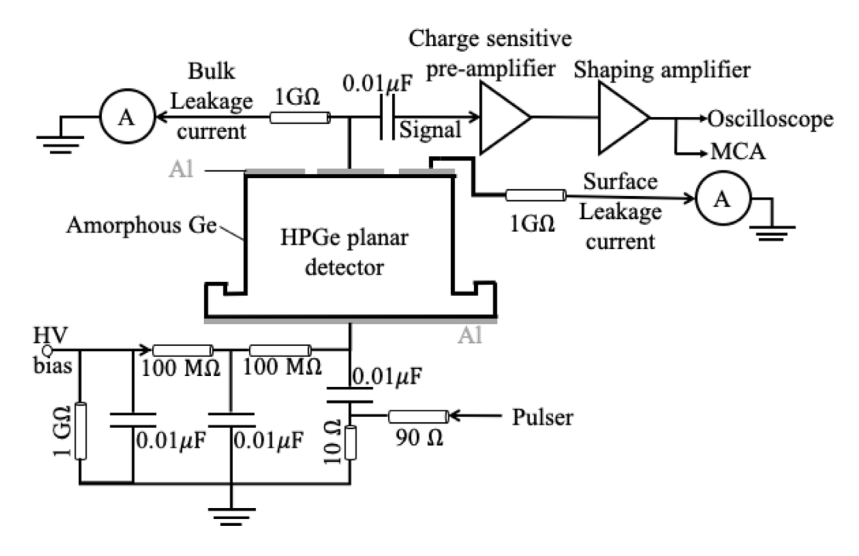


Fig. 2. Schematic representation of the electronic circuit for the characterization of a detector.

capacitance–voltage (C–V) characteristics [18–24]. In this study, we have used the I–V characteristics at different temperatures. We have also implemented a guard-ring structure on the top surface of the detector to separate the BLC from the SLC. The primary source of BLC is the injection of charge carriers from a-Ge contacts to the bulk of the detector. Though, thermal ionization of impurities is also a source of BLC [25], it is expected to be much smaller (~three orders of magnitude) than the injection from a-Ge contacts when the detector is operating at liquid nitrogen temperature (77 K). Therefore, the measured BLC as a function of bias voltage can be used to study the CBH at different temperatures.

2. Experimental methods

2.1. Fabrication of Ge detectors

Three guard-ring detectors made from p-type Ge crystals grown at University of South Dakota (USD) were used for the study of CBH. The crystals were grown using the Czochralski method [26,27]. High-purity Ge (HPGe) crystals were first sliced into small pieces with a diamond wire saw. Wings and grooves in a size of \sim 2 mm each were made on all of the four sides of the HPGe crystal as shown in Fig. 1. The purpose of the wings is to allow for handling the HPGe crystals, avoiding direct contact with the sensitive area of the crystal during the fabrication. HPGe crystals were lapped carefully to remove the visible scratches and chips that occur during the cutting process from a diamond saw. Silicon carbide (SiC) and aluminum oxide (Al₂O₃) powder with 17.5

and 9.5 μm grids, respectively, were used for lapping. The lapped crystals were then etched in a mixture (1:4) of hydrofluoric (HF) and nitric (HNO $_3$) acids to etch away the fine scratches. The etched crystal was then submerged in deionized water and dried with nitrogen gas. The well-processed HPGe crystals were loaded into the sputtering chamber and a-Ge was deposited on the top and the side surfaces of the crystals. Argon and hydrogen gas mixture (93:7) was used to create the plasma maintaining the chamber pressure of $\sim\!14$ mTorr, which is generated and confined to the space containing a HPGe crystal. Then the crystal was flipped and the same process was duplicated for the bottom side. The thickness of the a-Ge was maintained $\sim\!600$ nm for all three detectors.

Subsequently, a layer of aluminum (Al) with a thickness of ~100 nm was deposited on all the sides of the crystal to form a low-resistance contact area using an electron-beam evaporator for the detector USD-R02. For the detector USD-R03 and USD-W03, the Al contacts were sputtered on using the sputtering machine. To sputter Al on the a-Ge surface, plasma was created using argon gas maintaining the chamber pressure of 3 mTorr. On the top surface, two contacts were formed by etching out the Al to separate the center contact from the guardring (surface) contact. This allows the BLC to be measured through the center contact and the SLC to be measured through the guardring contact. A tape mask was used to protect the Al layer. Then the detector was dipped into a 1% HF solution. The a-Ge was unscathed on all surfaces of the detector. The final contact structures are sketched in Figs. 1 and 2. The full details of the fabrication procedure of Ge

detectors and their characterization at USD is reported in the papers published by our group [28–31].

Note that the completed Ge layers for all three detectors were very uniform after lapping, polishing, and etching, since the same recipe was applied. Therefore, we expect that the completed Ge layer for all three detectors have similar uniformity. This allows us to study how much the inhomogeneous deposition of a-Ge layer during the sputtering process can influence the leakage current.

2.2. Detector characterization

The leakage current of each detector was measured in a vacuum cryostat at USD. The schematic representation of the detector characterization set up is shown in Figs. 2 and 3. To monitor the temperature of the detector, a temperature sensor was placed at the bottom of the Al stage. For the detector to be in thermal equilibrium with the Al stage, the measurements were carried out an hour after inserting in the cryostat when the temperature sensor shows the desired temperature.

The leakage current was measured with the combination of a transimpedance amplifier and a multimeter. The voltage signal from the multimeter was converted back to the current signal. The precision of the leakage current measurement from our current setup is 0.1 pA.

The detector with a guard-ring structure allows the characterization of leakage current to be divided into two components: (a) BLC and (b) SLC. The BLC is mostly dominated by the charge injection from the top and the bottom contacts whereas the SLC is the current created by the surface defects. The variation of the leakage current density versus square root of bias voltage is shown in Fig. 4 as an example. The plot shows that there are two distinguishable regions, which correspond to two different ranges of the applied bias voltage, 10–20 V and 30–70 V. This feature indicates the quantum mechanical properties of the charge carriers. At a lower bias voltage (10–20 V), the reflection coefficient of charge carriers is more pronounced at the boundary than that at a higher bias voltage (30–70 V). For the study of the CBH at different temperatures, we have only taken into account the BLC for the bias voltage in the range of 30–70 V where thermionic emission dominates.

2.3. Charge blocking contacts

Charge carriers are injected through the contacts. To maintain a low leakage current, charge blocking contacts are needed. Lithium-diffused (n^+) and boron-implanted (p^+) contacts block holes and electrons, respectively. Diffusion of lithium into the detector reduces the sensitive volume of the detector. Since the a-Ge has negligible diffusion into the Ge detector, the sensitive volume of the detector for rare event searches remains intact. Furthermore, the bi-polar blocking behavior of a-Ge eliminates the need for two different contacts at the top and the bottom of a Ge detector [15]. For a high purity p-type Ge detector passivated with a-Ge contacts and the electrodes formed by deposition of Al, if it is negatively biased from the bottom electrode, then the detector starts to deplete from the top and the BLC is primarily dominated by hole injection from the top contacts. Non-zero conductivity of a-Ge also contributes to the SLC influenced by the hopping conduction mechanism [33,34]. The charge collection in a Ge detector is usually carried out with a bias voltage that is a few hundred volts above the full depletion voltage at which the contribution to the BLC is from both the top and bottom contacts. Analysis of the properties of the charge blocking contacts thoroughly is necessary for the successful operation of the detector. The charge blocking contacts formed by a layer of a-Ge on a Ge crystal are characterized on the basis of: (a) the CBH with respect to crystalline Ge; (b) the thermal stability; (c) the ability of withstanding high bias voltage without breakdown; and (d) the surface inhomogeneity.

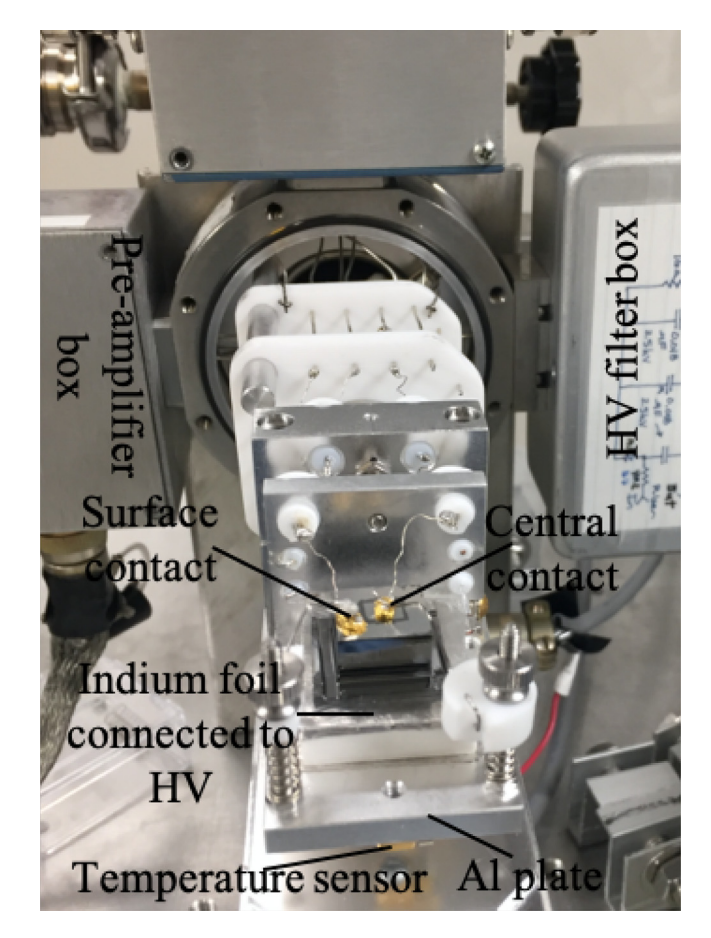


Fig. 3. Internal structure of the vacuum cryostat at USD.

2.4. I-V-T characteristics and CBH measurement

The CBH is calculated based on the current–voltage–temperature (I–V–T) characteristics. The saturation current is defined as the current density corresponding to zero bias voltage and can be obtained by extracting the linear portion of the logarithmic plot of current density versus bias voltage ($V \geq 3kT/q$). The model for the leakage current dependence on temperature and applied bias voltage is developed by Döhler, Brodsky [35–37] and Schottky [38]. This model was applied to a-Ge contacts on HPGe detectors as well [19]. Leakage current is directly proportional to temperature as reported in these studies [18, 19,29,35–40].

The thermionic emission model predicts the current flowing across the metal-semiconductor interface as:

$$J = J_{\infty} \exp(-\psi_{0,b}/kT)[1 - \exp(-qV_d/kT)]f(V_d), \tag{1}$$

where $f(V_d)=\exp\{([(2q(V_{bi}+V_d)+N/N_f)N/N_f]^{1/2}-N/N_f)/kT\}$, J is the ratio of leakage current to the contact area known as leakage current density, $\psi_{0,b}$ is the barrier height at zero bias voltage, k is the Boltzmann constant, T is temperature, V_{bi} is the built-in voltage, V_d is the bias voltage, N is the net impurity concentration, N_f is the density of localized energy states near the Fermi level. J_∞ equals to A^*T^2 in the case of a metal contact made on crystalline semiconductor and A^* is the effective Richardson constant. Since electric field penetration through the contacts is negligible when the bias voltage is low, the value of $f(V_d)$ is usually close to 1. It is worth mentioning that J_∞ can be replaced by $J_\infty = J_0T^2$ [32]. If the $V_d \gg V_{bi}$, or kT/q, or N/qN_f Eq. (1) reduces to

$$J = J_0 T^2 \exp(-\psi_{0,b}/kT) \exp[(2qV_d N/N_f)^{1/2}/kT]$$
 (2)

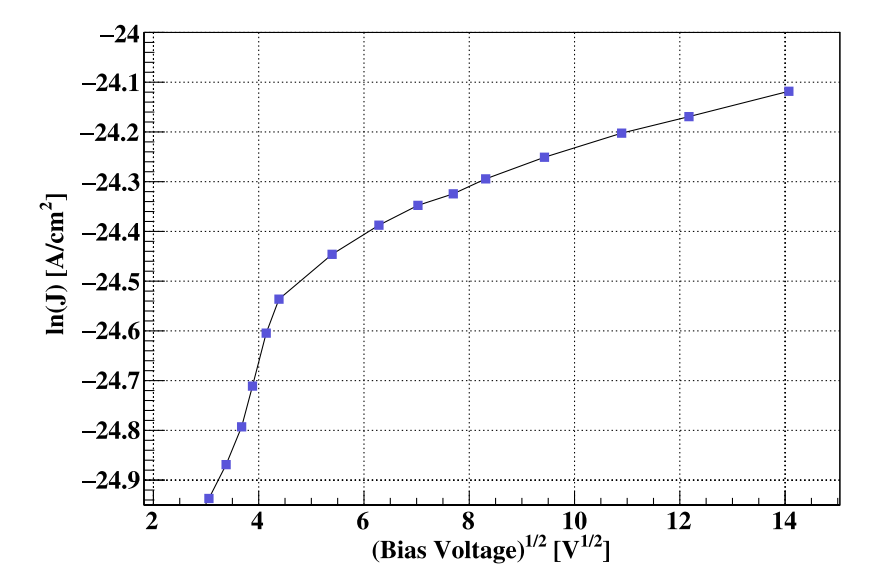


Fig. 4. The variation of the current density versus the square root of bias voltage for USD-R03 detector at 90 K. The plot shows that there are two distinguishable regions, which correspond to two different ranges of the applied bias voltage, 10-20 V and 30-70 V.

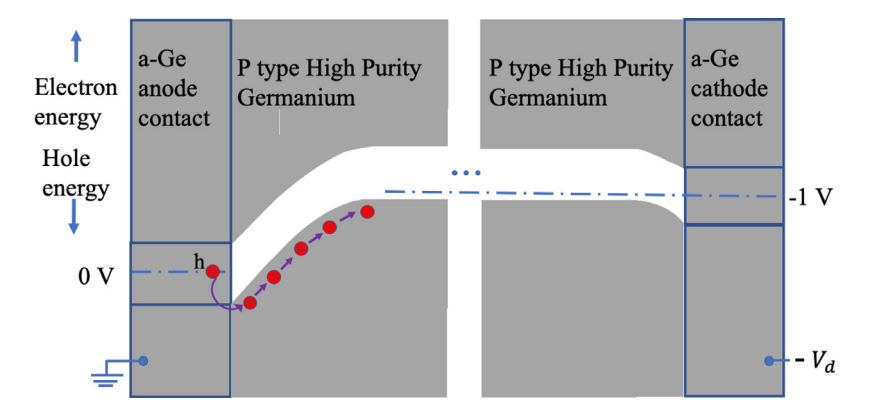


Fig. 5. Schematic representation of energy diagram when a small reverse bias is applied to the bottom contact of the p-type Ge detector [32] (not to scale).

for a partially-depleted detector. $\Delta \psi = \sqrt{2qV_dN/N_f}$ is the barrier lowering term. $\Delta \psi$ is directly proportional to the applied bias voltage, impurity concentration, and inversely to the density of defect states near the Fermi level. Therefore, to keep the barrier lowering value at a minimum, the density of localized energy states near the Fermi level should be high and the impurity concentration should be low. J_0 is a constant, the pre-factor, which is left as an open parameter to be determined from the measurements [32]. To calculate J_0 from Eq. (2), the barrier height should be treated as constant with respect to temperature. However, several pioneers have clearly demonstrated that the barrier height is not constant with temperature [41–47]. Such a phenomenon indicates there is a barrier inhomogeneity at the interface of a-Ge and crystalline Ge.

In order to study the variation of CBH as a function of temperature in the a-Ge contacts created at USD, we have treated the prefactor as constant and equal to the effective Richardson constant (48 $A/cm^{-2}~K^{-2}$) in the case of the a-Ge deposition on the p-type crystalline Ge [18] and have determined the barrier height at different temperatures.

Utilizing J_0T^2 equals A^*T^2 (A^* is the effective Richardson constant), Eq. (2) can be re-written as

$$J = A^*T^2 \exp(-\psi_{0,b}/kT) \exp[(2qV_dN/N_f)^{1/2}/kT]. \tag{3}$$

The Y-intercept obtained from the plot of lnJ versus the square root of the reverse bias voltage gives the saturation current density and is given by

$$J_s = A^* T^2 \exp{-(\psi_{0,h}/kT)}. (4)$$

The zero-bias barrier height can be expressed as:

$$\psi_{0,b} = kT \ln(J_s/A^*T^2). \tag{5}$$

Since A* = 48 A/cm⁻² K⁻² is a constant, thus, we can calculate $\psi_{0,b}$ for a given temperature using Eq. (4). Fig. 5 exhibits the energy band diagram for an interface between a layer of a-Ge and a p-type Ge crystalline structure. The variation of the zero-bias barrier height as a function of temperature indicates the inhomogeneity of the coated a-Ge layer.

It is worth pointing out that the slope obtained from the plot of $\ln J$ versus the square root of the reverse bias gives the density of localized energy states near the Fermi energy level for the a-Ge layer sputtered onto a-Ge surface for a given detector at a given temperature. The relationship between N_f and temperature can also be used to study the properties of the a-Ge layer, for example, the resistance or conductivity. However, it does not directly relate to the zero-bias barrier height, as described in Eq. (3). It may contribute to the systematic errors of the zero-bias barrier height in an indirect way, which is complicated and beyond the scope of this paper.

As an example, the variation of the BLC density versus the square root of bias voltage for USD-R03 detector is shown in Fig. 6 at the temperatures 90 K, 95 K, 100 K, 105 K and 110 K. Similar I-V-T characteristics were obtained for USD-R02 and USD-W03 detectors.

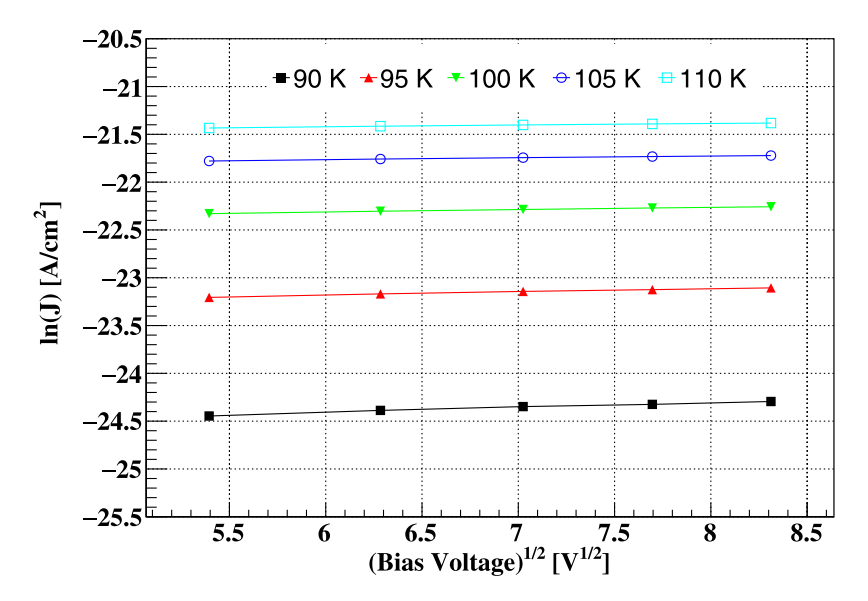
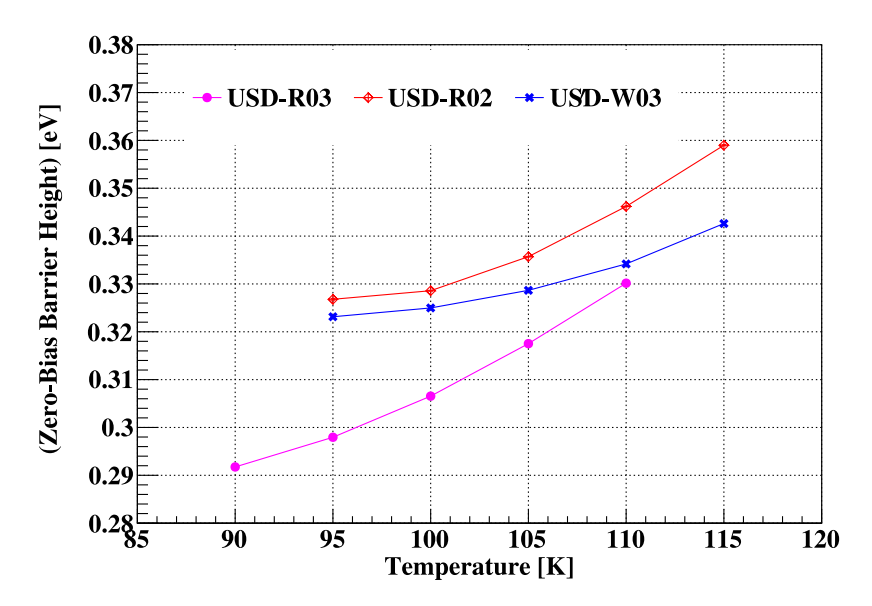


Fig. 6. The variation of the leakage current density versus the square root of bias voltage for USD-R03 detector at different temperatures.



 $\textbf{Fig. 7.} \ \ \textbf{The variation of the zero-bias barrier height versus temperature for three detectors.}$

The Y-intercept obtained from the plots gives the zero-bias BLC density which was used to calculate the zero-bias barrier height. Fig. 7 displays the dependence of calculated barrier height versus temperature for three detectors. When temperature increases, the barrier height increases or vice versa.

Note that there is a tendency that the zero-bias barrier height seem to saturate to a value above 0.32 eV for USD-R02 and USD-W03. The zero-bias barrier height seems to saturate to a value above 0.29 eV for USD-R03.

2.5. The relation between the inhomogeneity of a-Ge layer and CBH

A homogeneous interface layer allows us to predict the BLC at different temperature and applied bias voltage using Eq. (2), since the barrier height is a constant. However, for an inhomogeneous interface layer, the barrier height cannot be treated as a constant value with respect to temperature. The analysis of the I–V–T characteristics for three different detectors shows that the variation of CBH with respect to temperature is governed by the inhomogeneities at the interface of a-Ge and crystalline Ge. The existence of inhomogeneity at the interface

might be related to the cleanliness of the surface of crystalline Ge, the vacuum level inside the sputtering chamber, the stability of the gas flow while creating the plasma, and the variation in the thickness of a-Ge layer.

The vacuum pressure of the chamber for all three detectors was maintained less than 4×10^{-6} Torr. However, the gas flow rate was not stable. The pressure of the argon and hydrogen gas mixture in the chamber jumps between 12–16 mTorr. The instability of the chamber pressure during the plasma formation caused the unstable condition for the reflected power in the radio-frequency sputtering machine. Exposure to air during fabrication of the detector will be monitored in future detector fabrications to study its role in the nature of charge barrier.

The Gaussian distribution model developed by Werner and Guttler was applied to explain the correlation between the barrier height variation and the inhomogeneities of the interface [48]. The expression of the Gaussian model is described as:

$$\psi_{0,b} = \overline{\psi} - \sigma^2 / 2kT,\tag{6}$$

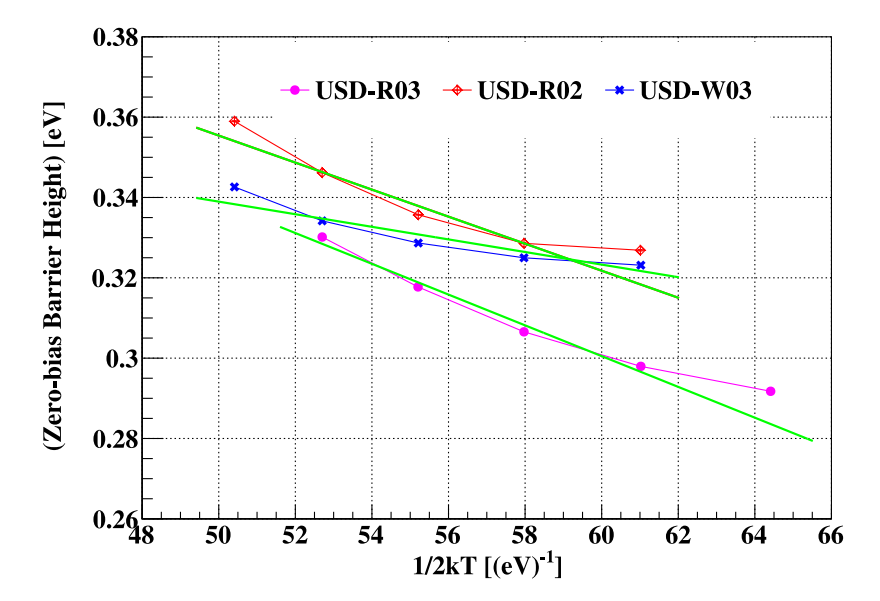


Fig. 8. The variation of zero-bias barrier height with 1/2kT for three detectors and the linear fit of it represented by the green line.

 Table 1

 Summary of three USD detector properties.

Detector	USD-R02	USD-R03	USD-W03
^a Impurity/cm ³	2.93×10^{10}	3.78×10^{10}	2.60×10^{10}
Thickness/cm	0.65	0.81	0.94
bArea/cm ²	0.29	0.48	0.24
$^{\rm c}V_{fd}/{ m V}$	700	1400	1300
$^{\rm d}\psi_{0,b}/{\rm eV}$ @90 K	_	$0.29174 \pm 1.8E - 4$	_
$^{\rm d}\psi_{0,b}/{\rm eV@95~K}$	$0.32679 \pm 1.8E - 4$	$0.29795 \pm 9.7E - 5$	$0.32313 \pm 1.3E - 4$
$^{\rm d}\psi_{0,b}/{\rm eV@100~K}$	$0.32858 \pm 9.3E - 5$	$0.30655 \pm 5.4E - 5$	$0.32498 \pm 1.5E - 4$
$^{\rm d}\psi_{0,b}/{\rm eV@105~K}$	$0.33570 \pm 6.4E - 5$	$0.31752 \pm 5.4E - 5$	$0.32866 \pm 1.6E - 4$
$^{\rm d}\psi_{0,b}/{\rm eV@110~K}$	$0.34619 \pm 6.7E - 5$	$0.33015 \pm 5.3E - 5$	$0.33418 \pm 1.8E - 4$
$^{\rm d}\psi_{0,b}/{\rm eV}@115~{\rm K}$	$0.35898 \pm 1.2E - 4$	-	$0.34262 \pm 2.4E - 4$
e ψ /eV	$0.52367 \pm 8.2E - 4$	$0.52359 \pm 8.3E - 4$	$0.41734 \pm 1.1E - 3$
$f\sigma^2/(eV)^2$	$0.00336 \pm 1.5E - 5$	$0.00371 \pm 1.4E - 5$	$0.00156 \pm 2.7E - 5$

^aNet impurity concentration calculated from the C-V measurements.

where $\overline{\psi}$ is the mean barrier height and σ is the standard deviation. σ is assumed to be a constant with respect to temperature for this calculation. The Y-intercept of the plot in Fig. 8 gives the value of $\overline{\psi}$ and the slope determines the value of σ^2 , respectively. The values of $\overline{\psi}$ and σ^2 for three detectors are shown in Table 1. As can be seen from Table 1, the value of σ is smaller for USD-W03 detector, which indicates the barrier height fluctuation is smaller than the other two detectors. This implies that the variation of the BLC from USD-W03 will be less than the other two detectors when increasing or decreasing temperature. The standard deviation measured from the Gaussian distribution of barrier height indicates that the barrier inhomogeneity cannot be neglected while calculating the barrier height. The deviation of σ with respect to $\overline{\psi}$ is within the range of 9%–12% for all the detectors that were used for this study.

For an ideal case, when σ^2 is close to 0, the sum of electron barrier height (ϕ_e) and hole barrier height (ϕ_h) equal to the band-gap of Ge [40]. The barrier height for electrons or holes was obtained from the slope of the leakage current density after the detector was fully depleted assuming the constant barrier height at two different temperatures. However, the sum of $\phi_e + \phi_h$ equals to the band-gap of Ge may not be accurate to describe the real case since it does not consider the barrier height fluctuation due to the inhomogeneities.

It is worth mentioning that the Gaussian model is used to study the barrier inhomogeneity. A smaller value of σ indicates a more

homogeneous barrier and hence pointing to a better sputtering process in the fabrication of a-Ge contacts. Since the value of σ^2 indicates the inhomogeneity of CBH, which is related to the fabrication process, we expect to improve the fabrication process to keep the value of σ^2 as small as possible. A low value of σ^2 also implies that the better rectifying contacts are formed which are closed to ideal thermionic case [49].

Table 1 summarizes the properties of the a-Ge contacts deposited on the HPGe crystal grown at USD.

3. Conclusions

For the first time, this study focuses on the CBH variation with respect to temperature for a-Ge deposited on crystalline Ge. Barrier height for the same detectors used in this study was calculated assuming constant barrier height without considering the inhomogeneity in our previous publication [18]. However, this model fails to accurately predict the leakage current for a wide range of temperatures. The prefactor which depends on the process parameters was left as an open parameter and it is different for each detector. In this study the prefactor (J_0) is treated as the effective Richardson constant (A^*) to study the inhomogeneity of interface layer. Thus, the level of inhomogeneity of the interface layer between a-Ge and Ge for each detector is attributed to the process parameters of fabricating Ge detectors.

^bArea of the central contact on the top surface.

^cFull depletion voltage for the detector.

^dZero-bias barrier height.

^eMean-barrier height.

^fVariance of barrier height fluctuation.

The variation of the barrier height at different temperatures has been explained by considering the Gaussian distribution model. The inhomogeneity of a-Ge contacts created on the crystalline surface is the main source of barrier height fluctuation with respect to temperature. The observed inhomogeneity difference in the a-Ge layers from three USD detectors suggests that the fabrication process can be improved to obtain a smaller variation in the barrier height for rare-event physics searches.

CRediT authorship contribution statement

Rajendra Panth: Data curation, Formal analysis, Detector fabrication. Wenzhao Wei: Detector fabrication. Dongming Mei: Conceptualization, Methodology. Jing Liu: Equipment and electronics. Sanjay Bhattarai: Crystal growth. Hao Mei: Crystal growth. Mathbar Raut: Crystal growth. Pramod Acharya: Zone refining. Kyler Kooi: Zone refining. Guojian Wang: Crystal growth.

Declaration of competing interest

The authors declare that they have no known competing financial interests or personal relationships that could have appeared to influence the work reported in this paper.

Acknowledgments

The authors would like to thank Mark Amman for his instruction on fabricating planar detectors, and the Nuclear Science Division at Lawrence Berkeley National Laboratory for providing the vacuum cryostat. We would also like to thank Christina Keller for a careful reading of this manuscript. This work was supported by NSF OISE-1743790, PHYS-1902577, OIA-1738695, DOE FG02-10ER46709, the Office of Research at the University of South Dakota and a research center supported by the State of South Dakota.

References

- M.S. Amman, P.N. Luke, Position-sensitive germanium detectors for gamma-ray imaging and spectroscopy, in: Hard X-Ray, Gamma-Ray, and Neutron Detector Physics II, 4141, 2000.
- [2] R.H. Phel, Germanium gamma-ray detectors, 1977.
- [3] A.J. Tavendale, Large germanium lithium-drift pin diodes for gamma-ray spectroscopy, IEEE Trans. Nucl. Sci. 12 (1) (1965) 255–264.
- [4] A.H. Muggleton, Semiconductor devices for gamma ray, X ray and nuclear radiation detection, J. Phys. E: Sci. Inst. 5 (5) (1972) 390.
- [5] M. Agostini, et al., Searching for neutrinoless double beta decay with GERDA, J. Phys. Conf. Ser. 1342 (1) (2020).
- [6] S.I. Alvis, et al., Search for neutrinoless double-β decay in Ge 76 with 26 kg yr of exposure from the Majorana Demonstrator, Phys. Rev. C 100 (2) (2019) 025501
- [7] N. Abgrall, et al., The large enriched germanium experiment for neutrinoless double beta decay (LEGEND), AIP Conf. Proc. 1894 (1) (2017).
- [8] C.E. Aalseth, et al., CoGeNT: A search for low-mass dark matter using p-type point contact germanium detectors, Phys. Rev. D 88 (1) (2013) 012002.
- [9] Y. Wang, et al., Improved limits on solar axions and bosonic dark matter from the CDEX-1B experiment using the profile likelihood ratio method, Phys. Rev. D 101 (5) (2020) 052003.
- [10] R. Agnese, et al., Results from the super cryogenic dark matter search experiment at Soudan, Phys. Rev. Lett. 120 (6) (2018) 061802.
- [11] D.-M. Mei, et al., Direct detection of MeV-scale dark matter utilizing germanium internal amplification for the charge created by the ionization of impurities, Eur. Phys. J. C 78 (3) (2018) 1–12.
- [12] C.E. Aalseth, et al., Astroparticle physics with a customized low-background broad energy Germanium detector, Nucl. Instrum. Methods Phys. Res. A 652 (1) (2011) 692–695.
- [13] B.H. Hasegawa, et al., A prototype high-purity germanium detector system with fast photon-counting circuitry for medical imaging, Med. Phys. 18 (5) (1991) 900–909.
- [14] S. Stave, Germanium detectors in homeland security at PNNL, J. Phys. Conf. Ser. 606 (1) (2015).

- [15] P.N. Luke, et al., Amorphous Ge bipolar blocking contacts on Ge detectors, IEEE Trans. Nucl. Sci. 39 (4) (1992) 590–594.
- [16] P.N. Luke, R.H. Pehl, F.A. Dilmanian, A 140-element Ge detector fabricated with amorphous Ge blocking contacts, IEEE Trans. Nucl. Sci. 41 (4) (1994) 976–978.
- [17] P.N. Luke, et al., Germanium orthogonal strip detectors with amorphoussemiconductor contacts, IEEE Trans. Nucl. Sci. 47 (4) (2000) 1360–1363.
- [18] W.-Z. Wei, et al., The impact of the charge barrier height on germanium (Ge) detectors with amorphous-Ge contacts for light dark matter searches, Eur. Phys. J. C 80 (2020) 1–10.
- [19] E.L. Hull, R.H. Pehl, Amorphous germanium contacts on germanium detectors, Nucl. Instrum. Methods Phys. Res. A 538 (1–3) (2005) 651–656.
- [20] S.K. Tripathi, M. Sharma, Analysis of the forward and reverse bias IV and CV characteristics on Al/PVA: n-PbSe polymer nanocomposites Schottky diode, J. Appl. Phys. 111 (7) (2012) 074513.
- [21] T. Zhang, C. Raynaud, D. Planson, Measure and analysis of 4H-SiC schottky barrier height with Mo contacts, Eur. Phys. J. Appl. Phys. 85 (1) (2019) 10102.
- [22] H. Sheoran, et al., Temperature-dependent electrical characteristics of Ni/Au vertical Schottky barrier diodes on β -Ga2O3 epilayers, ECS J. Solid State Sci. Technol. 9 (5) (2020) 055004.
- [23] R. Nouchi, Extraction of the schottky parameters in metal-semiconductor-metal diodes from a single current-voltage measurement, J. Appl. Phys. 116 (18) (2014) 184505.
- [24] A. Di Bartolomeo, et al., Tunable Schottky barrier and high responsivity in graphene/Si-nanotip optoelectronic device, 2D Mater. 4 (1) (2016) 015024.
- [25] W.L. Hansen, E.E. Haller, Amorphous germanium as an electron or hole blocking contact on high-purity germanium detectors, IEEE Trans. Nucl. Sci. 24 (1) (1977) 61–63
- [26] G.-J. Wang, et al., Crystal growth and detector performance of large size high-purity Ge crystals, Mater. Sci. Semicond. Process. 39 (2015) 54–60.
- [27] G.-J. Wang, et al., High purity germanium crystal growth at the university of South Dakota, J. Phys. Conf. Ser. 606 (1) (2015).
- [28] X.-H. Meng, et al., Fabrication and characterization of high-purity germanium detectors with amorphous germanium contacts, J. Instrum. 14 (02) (2019) P02019.
- [29] W.-Z. Wei, et al., Investigation of amorphous germanium contact properties with planar detectors made from USD-grown germanium crystals, J. Instrum. 13 (12) (2018) P12026.
- [30] D.-M. Mei, et al., Impact of charge trapping on the energy resolution of Ge detectors for rare-event physics searches, J. Phys. G: Nucl. Part. Phys. 47 (10) (2020) 105106.
- [31] M.-S. Raut, et al., Characterization of high-purity germanium (Ge) crystals for developing novel Ge detectors, J. Instrum. 15 (10) (2020) T10010.
- [32] M. Amman, Optimization of amorphous germanium electrical contacts and surface coatings on high purity germanium radiation detectors, 2018, arXiv preprint, arXiv:1809.03046.
- [33] T. Shutt, et al., A solution to the dead-layer problem in ionization and phonon-based dark matter detectors, Nucl. Instrum. Methods Phys. Res. A 444 (1–2) (2000) 340–344.
- [34] S. Bhattarai, et al., Investigation of the electrical conduction mechanisms in P-type amorphous germanium electrical contacts for germanium detectors in searching for rare-event physics, Eur. Phys. J. C 80 (10) (2020) 1–10.
- [35] G.H. Doöhler, M.H. Brodsky, Amorphous-crystalline heterojunctions, AIP Conf. Proc. 20 (1) (1974).
- [36] M.H. Brodsky, G.H. Döhler, P.J. Steinhardt, On the measurement of the conductivity density of states of evaporated amorphous silicon films, Phys. Status Solidi (B) 72 (2) (1975) 761–770.
- [37] M.H. Brodsky, G.H. Doöhler, A new type of junction: Amorphous/crystalline, Crit. Rev. Solid State Mater. Sci. 5 (4) (1975) 591–595.
- [38] S.M. Sze, Y. Li, K.K. Ng, Physics of Semiconductor Devices, John wiley and sons, 1981.
- [39] R. Panth, et al., Characterization of high-purity germanium detectors with amorphous germanium contacts in cryogenic liquids, Eur. Phys. J. C 80 (7) (2020) 1–11.
- [40] Q. Looker, M. Amman, K. Vetter, Leakage current in high-purity germanium detectors with amorphous semiconductor contacts, Nucl. Instrum. Methods Phys. Res. A 777 (2015) 138–147.
- [41] S. Zeyrek, et al., The double gaussian distribution of inhomogeneous barrier heights in Al/GaN/p-GaAs (MIS) schottky diodes in wide temperature range, Braz. J. Phys. 38 (2008) 591–597.
- [42] S. Toumi, et al., Gaussian distribution of inhomogeneous barrier height in tungsten/4H-SiC (000-1) Schottky diodes, Microelectron. Eng. 86 (3) (2009) 303–309.
- [43] S. Sil, et al., Elucidation of inhomogeneous heterojunction performance of Al/Cu 5 FeS 4 Schottky diode with a Gaussian distribution of barrier heights, IEEE Trans. Electron Devices 67 (5) (2020) 2082–2087.

- [44] J. Nicholls, et al., Description and verification of the fundamental current mechanisms in silicon carbide Schottky barrier diodes, Sci. Rep. 9 (1) (2019) 1-9.
- [45] W.C. Huang, et al., Barrier heights engineering of Al/p-Si Schottky contact by a thin organic interlayer, Microelectron. Eng. 107 (2013) 200–204.
- [46] K. Zeghdar, et al., Inhomogeneous barrier height effect on the current–voltage characteristics of an Au/n-InP Schottky diode, J. Semiconductors 36 (12) (2015) 124002.
- [47] S. Karboyan, J.-G. Tartarin, B. Lambert, Analysis of barrier inhomogeneities in AlGaN/GaN HEMTs' Schottky diodes by IVT measurements, in: 2013 European Microwave Integrated Circuit Conference, IEEE, 2013.
- [48] J.H. Werner, H.H. Güttler, Barrier inhomogeneities at Schottky contacts, J. Appl. Phys. 69 (3) (1991) 1522–1533.
- [49] W. Mtangi, et al., Analysis of temperature dependent I–V measurements on Pd/ZnO Schottky barrier diodes and the determination of the Richardson constant, Physica B 404 (8–11) (2009) 1092–1096.